PSF Dedicated to Estimation of Displacement Vectors for Tissue Elasticity Imaging with Ultrasound

Hervé Liebgott, Jens E. Wilhjelm, *Member, IEEE*, Jørgen A. Jensen, *Senior Member, IEEE*, Didier Vray, *Member, IEEE*, and Philippe Delachartre

***Abstract*—This paper investigates a new approach devoted to displacement vector estimation in ultrasound imaging. The main idea is to adapt the image formation to a given displacement estimation method to increase the precision of the estimation. The displacement is identified as the zero crossing of the phase of the complex cross-correlation between signals extracted from the lateral direction of the ultrasound RF image. For precise displacement estimation, a linearity of the phase slope is needed as well as a high phase slope. Consequently, a particular point spread function (PSF) dedicated to this estimator is designed. This PSF, showing oscillations in the lateral direction, leads to synthesis of lateral RF signals. The estimation is included in a 2-D displacement vector estimation method. The improvement of this approach is evaluated quantitatively by simulation studies. A comparison with a speckle tracking technique is also presented. The lateral oscillations improve both the speckle tracking estimation and our 2-D estimation method. Using our dedicated images, the precision of the estimation is improved by reducing the standard deviation of the lateral displacement error by a factor of 2 for speckle tracking and more than 3 with our method compared to using conventional images. Our method performs 7 times better than speckle tracking. Experimentally, the improvement in the case of a pure lateral translation reaches a factor of 7. Finally, the experimental feasibility of the 2-D displacement vector estimation is demonstrated on data acquired from a Cryogel phantom.**

I. Introduction

Tissue elasticity imaging with ultrasound deals with the mapping of any parameter characterizing the elastic properties of a given medium using ultrasound echo data. There are different ways to do tissue elasticity imaging with ultrasound which differ by the way the tissue under investigation is excited. It is important to make a distinction between the static approaches and the dynamic ones. Dynamic excitation of the tissue can be made by a dynamic vibration, which is normally referred to as sonoelastography [1], [2], or by a pulsed low frequency vibration, which is normally referred to as transient elastography [3], [4]. In this paper we will focus on the static approach, also called elastography, as it has been introduced by Ophir *et al.* [5]. Here the principle is to estimate the local displacement or the strain field between two ultrasound images of a medium. The two images are acquired at two different static compression states. Elasticity has been shown to be a good candidate for characterization of the development of different pathologies [6], [7].

The early approaches to elastography have been attempts to characterize the tissue elasticity by simply considering the axial strain image. If the applied stress is axial, it is this direction that features the largest strain. However, knowledge of only one component of the strain field is not enough to provide a precise and quantitative investigation of the medium [8]. As a consequence, a number of methods have been used to estimate the lateral component of the displacement field [9]–[11].

To estimate the displacement, it is possible to use the phase of the complex cross-correlation between signals from a reference image and from an image obtained after compression of the medium (also called the displaced image). Indeed, this phase has the feature of being null for the right displacement, and it can be found easily using, for example, the Newton method. This feature has been used with success for axial displacement estimation [12]. More recently, this feature has also been used for lateral displacement estimation based on conventional ultrasound RF images [13]. However, as it will be shown in this paper, the quality of this estimation method can be improved by taking into account the image formation method, and using a new, dedicated point spread function (PSF). Indeed, with conventional RF images, neither the complex correlation phase linearity nor the phase slope is controlled. The phase slope is directly related to the precision of the estimated displacement.

This work proposes a method to improve the precision of the estimation of the lateral component of the displacement. To reach this goal, a specific PSF dedicated to lateral displacement estimation by means of the phase of the complex correlation function is designed. The starting point is the expression of the correlation function, which is chosen to have a linear phase. Then, it is shown analytically that having a constraint of linear phase leads to a specific

Manuscript received March 3, 2006; accepted November 20, 2006.

H. Liebgott is with CREATIS-LRMN, CNRS, UMR5220, INSERM, U630, Université Lyon 1, F-6900, France (e-mail: liebgott@creatis.univ-lyon1.fr).

D. Vray and P. Delachartre are with CREATIS, CNRS-LRMN, UMR5220, INSERM, U630, INSA Lyon, F-69621, France.

J. E. Wilhjelm is with the Center for Arteriosclerosis Detection with Ultrasound, The Technical University of Denmark, DK-2800 Kgs Lyngby, Denmark.

J. A. Jensen is with the Center for Fast Ultrasound imaging, The Technical University of Denmark, DK-2800 Kgs Lyngby, Denmark.

Digital Object Identifier 10.1109/TUFFC.2007.308

expression of the lateral profile of the PSF. This lateral profile showing oscillations is characterized by two parameters, the width and the wavelength of the oscillations. The width of the PSF is related to the spatial resolution of the ultrasound images, and the wavelength of the oscillations is related to the precision of the displacement estimation. Those parameters can be controlled by receive beamforming.

The paper will proceed as follows. First, a simple image model is presented together with the method for beamformer design. Then the lateral displacement estimation method and the displacement vector estimation scheme are introduced. Simulation results showing the improvement when using the new dedicated images for lateral displacement estimation compared to conventional images are presented. Experimental results showing the feasibility and improvement in a real situation are given. A discussion of the results and a conclusion are finally provided.

II. Image Model, PSF, Beamforming

The formation of an ultrasound RF image $r(x, y)$ can be described by a linear relation involving the impulse response of the imaging system, also called the PSF, $h(x, y)$, and a discrete distribution of scatterers representing the medium, $d(x, y)$. If only two spatial dimensions are considered, this can be written as a convolution over the lateral and axial spatial variables x and y, respectively. The convolution is denoted $\otimes_{x,y}$. This can be written

$$r(x, y) = h(x, y) \underset{x,y}{\otimes} d(x, y). \tag{1}$$

The scatterer distribution,

$$d(x, y) = \sum_i A_i \delta(x - x_i,\, y - y_i), \tag{2}$$

is assumed to be spatially uncorrelated. In (2), A_i represents the ith scatterer strength or echogeneity and $\{x_i,\, y_i\}$ its position. The PSF $h(x, y)$ is considered separable in the spatial dimensions [14] as

$$h(x, y) = h_x(x) h_y(y), \tag{3}$$

where $h_y(y)$ is related to the excitation pulse and the impulse response of the elements of the probe, and $h_x(x)$ is related to diffraction and interferences between contributions from all transducer elements [15]. This assumption will be used for the PSF design.

With this model, it is easy to show that the image of a translated medium is a translated version of the initial (reference) image in a region $(x, y) \in \Omega$, where the shape of the PSF and the displacement vector are assumed constant. For such a constant displacement, $(\Delta x,\, \Delta y)$, the new image $s(x, y)$, which can also be called the displaced image, is simply related to the reference image $r(x, y)$ by

$$s(x, y) = r(x - \Delta x,\, y - \Delta y). \tag{4}$$

III. Displacement Estimation Method

A. Design of a PSF Dedicated to Lateral Displacement Estimation

In this work, a specific PSF is used to increase the quality of the displacement estimation. A specific shape of the PSF, and in particular its lateral profile, can be obtained by beamforming techniques, in different ways. In a previous paper [16], we have described a beamformer design method based on a Fraunhoffer approximation, which will be used here. A plane wave is emitted and the received raw signals are processed dynamically using quadratic focusing and a dynamic apodization function equal to the inverse Fourier transform of the expected lateral PSF profile. This approach has previously been used by others [17].

In this subsection, the estimation method is described and it is shown how the choice of this estimation method leads to the use of a particular PSF and, as a consequence, a particular apodization function.

Here, the phase of the complex correlation function between displaced versions of a given signal is studied. This phase has the feature of being null at the value of the displacement. The imaginary part of the complex signals used to calculate the correlation function is calculated as the Hilbert transform of the real signals. When the estimation is done in the axial direction, the Hilbert transform is calculated in the axial direction; when the lateral direction is considered, the Hilbert transform is calculated in the lateral direction.

First, the lateral direction of the image is considered. The signals considered are composed of samples coming from the same depth in the RF image. Those signals are limited in size and the following derivations have to be considered locally. One signal is extracted from the reference image and one from the displaced image. They are considered to be displaced versions of each other. To find the right displacement between the two signals, the location of the zero crossing of the phase of the complex correlation between the two lateral RF signals is estimated.

The shape of the lateral profile of the PSF is calculated analytically starting from the expression of the complex correlation between reference and displaced signals. To facilitate the estimation and to improve its quality, the phase of the complex correlation function is chosen to be linear. As there is no particular expectation about the magnitude of the complex correlation function, it is chosen as Gaussian because it is easily obtained, easily manipulated analytically, and fairly close to a realistic situation. The complete expression of the complex correlation function, as a function of spatial shift X, is given by

$$\tilde{R}_{rs}(X) = \frac{\sigma_u}{\sqrt{2}} e^{-\pi \left(\frac{\sigma_u}{\sqrt{2}}(X - \Delta x)\right)^2} e^{-j2\pi \frac{1}{\lambda_x}(X - \Delta x)}, \tag{5}$$

where Δx is the lateral displacement that has to be estimated, $1/\lambda_x$ is the slope of the phase, and $\sqrt{2}/\sigma_u$ is the full width at half maximum (FWHM) of the Gaussian envelope. The expression of the Gaussian is chosen so that

the following mathematical manipulations lead to simplifications of the expression. The autocorrelation function is given for $\Delta x = 0$ as

$$\tilde{R}_{rr}(X) = \frac{\sigma_u}{\sqrt{2}} e^{-\pi\left(\frac{\sigma_u}{\sqrt{2}}X\right)^2} e^{-j2\pi\frac{1}{\lambda_x}X}. \quad (6)$$

It is possible to calculate the power spectral density of the complex lateral signal as the Fourier transform of the autocorrelation function

$$P_{\tilde{r}}(u) = F\left\{\tilde{R}_{rr}(X)\right\} = e^{-2\pi\left(\frac{u}{\sigma_u}\right)^2} \underset{u}{\otimes} \delta\left(u - \frac{1}{\lambda_x}\right), \quad (7)$$

where $F\{\,\}$ denotes the Fourier transform and u is the spatial frequency in m^{-1}. The magnitude of the Fourier transform of the complex signal, denoted $A_{\tilde{r}}(u)$, is equal to the square root of the power spectral density

$$A_{\tilde{r}}(u) = e^{-\pi\left(\frac{u}{\sigma_u}\right)^2} \underset{u}{\otimes} \delta\left(u - \frac{1}{\lambda_x}\right). \quad (8)$$

And finally the magnitude spectrum of the corresponding real signal is

$$A_r(u) = \frac{1}{2} e^{-\pi\left(\frac{u}{\sigma_u}\right)^2} \underset{u}{\otimes} \left(\delta\left(u - \frac{1}{\lambda_x}\right) + \delta\left(u + \frac{1}{\lambda_x}\right)\right). \quad (9)$$

Because the scatterer distribution is spatially uncorrelated, its autocorrelation is a delta function and its spectrum is a uniform distribution. As the spectrum of the lateral signal is the product of the spectrum of the PSF and the spectrum of the scatterer distribution, there is no trace of the latter in the expression of the magnitude spectrum of the lateral signal. The magnitude spectrum of the lateral signal given in (9) is equal to the magnitude spectrum of the lateral profile of the PSF $A_h(u)$ as

$$A_r(u) = A_h(u). \quad (10)$$

As a consequence, the magnitude of the spectrum of the PSF $A_h(u)$ is equal to (9). The profile of the PSF is calculated by inverse Fourier transform of its spectrum. Because there is no expectation about the phase of this spectrum, a uniform phase has been chosen. The lateral profile of the PSF is equal to

$$h(x) = e^{-\pi\left(\frac{x}{\sigma_x}\right)^2} \cos\left(2\pi\frac{x}{\lambda_x}\right), \quad (11)$$

where x is the spatial variable associated with the lateral direction. Eq. (11) shows that the PSF has lateral oscillations, which can be compared to the PSF used in [17], which presents a method for blood flow estimation. In [17], the PSF was a sinusoid limited by a square window whereas here the window is Gaussian. As a consequence, the associated apodization functions are also different, specifically, Gaussians in our approach and sinc functions in [17]. Anderson has also studied this kind of PSF. Particularly in [18], different apodization functions, all leading to lateral oscillations, have been tested for 2-D velocity estimation.

The lateral signals extracted from RF images obtained with this PSF can be called lateral RF signals. The most convenient way to control the lateral profile of the PSF, as presented in [16] and [17], is to emit a plane wave, and then the lateral profile of the PSF can be controlled by receive beamforming only. The plane wave is produced by exciting all active elements at the same time. If dynamic quadratic focusing is used, the receive apodization function that leads to a given lateral PSF profile is its inverse Fourier transform. In this case, the apodization function is equal to the convolution of a Gaussian function of FWHM σ_0 with a distribution of two delta functions of position $\pm x_0$ as

$$w(x_i) = \frac{1}{2} e^{-\pi\left(\frac{x_i}{\sigma_0}\right)^2} \underset{x_i}{\otimes} \left(\delta(x_i - x_0) + \delta(x_i + x_0)\right). \quad (12)$$

Here, $w(x_i)$ is the weighting coefficient applied to the ith element which has lateral position x_i. According to the Fraunhoffer approximation, the relation between the apodization function parameters and those from the PSF are given by

$$x_0 = \frac{y\lambda}{\lambda_x}, \quad (13)$$

$$\sigma_0 = \frac{y\lambda\sqrt{2}}{\sigma_x}, \quad (14)$$

where λ is the wavelength of the emitted wave, y is the depth of interest, λ_x is the wavelength of the lateral oscillations, σ_x is the FWHM of the Gaussian envelope of the PSF, σ_0 is the FWHM of the Gaussian peaks of the apodization function, and x_0 their position. The PSF and apodization are illustrated in Fig. 1.

As can be seen in (13) and (14) both parameters of the apodization function are given as a function of the depth y. The apodization function must thus be adapted dynamically with respect to the depth while processing the raw received signals. The receive focusing is also adapted dynamically: dynamic quadratic focusing is used. This makes it possible to limit the size of the lateral PSF and to reach the Fraunhoffer approximation. Dynamic focusing and apodization are used in this work.

B. Aperture Function Parameters

The expression of the lateral profile of the PSF and the expression of the apodization function that leads to this particular PSF profile have been given in (11) and (12), respectively. The actual values of the key parameters, λ_x and σ_x, are limited by the physical size of the active part of the ultrasound probe.

Intuitively, a high oscillation frequency in the lateral direction would lead to a better displacement estimate because it increases the phase slope. If it is steeper, its zero crossing is identified more precisely. Moreover, a thin PSF

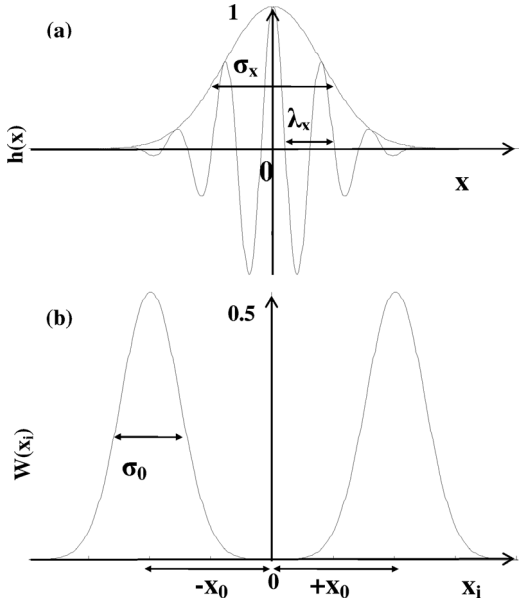

Fig. 1. (a) PSF profile and (b) apodization function. O is the origin of the coordinate system.

would lead to a better spatial resolution. Unfortunately, both improvements require an increase in the length of the active part of the probe and, with a constant pitch, a higher number of elements. A trade-off must be made between lateral resolution and phase slope which is related to estimator performance. This can be expressed quantitatively as a function of the parameters of the apodization function or as a function of the PSF parameters. In the present work, the apodization function is considered well defined if 99% of the area under its curve is inside the active part of the probe. In order to reach this requirement, the apodization function parameters must respect

$$1.2\sigma_0 + x_0 \leq \frac{W}{2}, \tag{15}$$

which can be expressed as a function of the PSF parameters as

$$1.2\frac{y\lambda\sqrt{2}}{\sigma_x} + \frac{y\lambda}{\lambda_x} \leq \frac{W}{2}, \tag{16}$$

where W is the length of the active part of the probe, and λ, λ_x, σ_x, σ_0, and x_0 are the same parameters as in (13) and (14).

To choose the optimal value of σ_x and λ_x with a given probe, a simple simulation was made. Three thousand different pairs of reference and strain signals were randomly generated. The probe simulated was a commercial linear array probe; its parameters are given in Table I. The probe was assumed to use 64 active elements, and, with a pitch of 0.208 mm, the active part of the probe is 13.3 mm long. The parameter set (σ_x, λ_x) was chosen so as to minimize the mean square error (MSE) between the true and the estimated displacements, over all realizations. For the simulation, the strain scatterer distribution was assumed to be

TABLE I
PARAMETERS OF THE COMMERCIAL PROBE USED.

Parameter	Value
Center frequency	7 MHz
Total number of elements	128
Number of active elements	64
Element height	4.5 mm
Element width	0.173 mm
Distance between two elements	0.035 mm

a stretched version of the reference scatterer distribution as follows

$$d'(x) = d\left(\left(1 + \frac{\varepsilon}{100}\right)x\right), \tag{17}$$

with ε, the strain, given as a percentage. As a consequence, the displacement of the scatterers is not the same for the whole length of the window. This is what happens in a real situation. The true displacement is considered to be the displacement of a scatterer situated in the middle of the window. The MSE is the average over the 3000 realizations of the squared difference between the true displacement Δ_{xi} and the estimated displacement $\widehat{\Delta}_{xi}$. It is expressed by

$$\text{MSE} = \frac{1}{N}\sum_{i=1}^{N}\left(\Delta_{xi} - \widehat{\Delta}_{xi}\right)^2, \tag{18}$$

where N is the total number of realizations.

Different values of λ_x and σ_x have been investigated and the result is reported in Fig. 2. More values than those that can be reached with our probe according to (16) have been tested. The tendency is a reduced mean quadratic error with a decrease of the lateral wavelength λ_x and a decrease of the width of the PSF σ_x, as would be expected intuitively. Finally, the parameters are chosen as follows: $\lambda_x = 2.6$ mm and $\sigma_x = 2.8$ mm. It is interesting to notice that the result could be improved somewhat more if the probe were larger.

C. System Architecture

To estimate the axial and lateral components of the displacement field, a 2-D displacement estimation method based on a twice-1-D scheme is used as follows, and as given in Fig. 3. The estimation is done locally using windows from the axial or lateral RF signals. For each local estimation, the displacement is identified with the zero crossing of the phase of the complex correlation which is estimated using the Newton method as described in [12]. An adapted windowing technique is used that takes into account the estimation previously done for neighboring points.

For each direction of estimation, a different set of images is used. The images obtained with the beamformer presented previously [dynamic quadratic focusing and apodization function given in (12)] show oscillations in both directions of space. This is not well suited to the

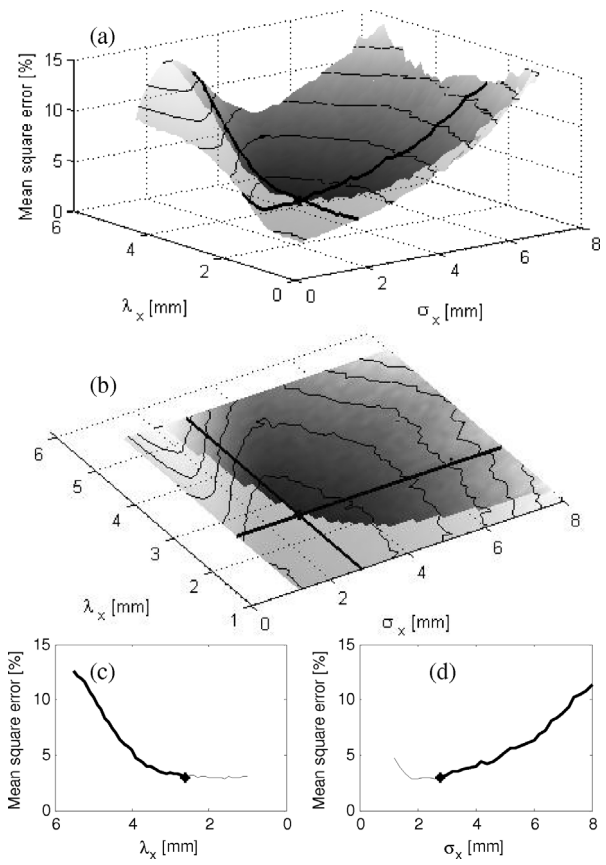

Fig. 2. Mean squared error as a function of λ_x and σ_x. The parameters that can not be reached with our probe are represented in semi-transparency on the 3-D plot (a) and on the projection (b), and by a thin line on the 2-D plots, (c) and (d). The dot indicates the optimum, which is for $\lambda_x = 2.6$ mm and $\sigma_x = 2.8$ mm. The plots correspond to the two black lines on the 3-D plot, and on the projection.

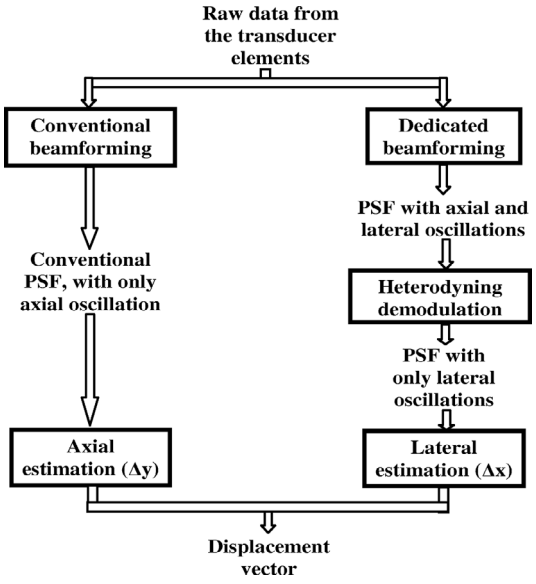

Fig. 3. Sketch for using specific images for each direction of estimation.

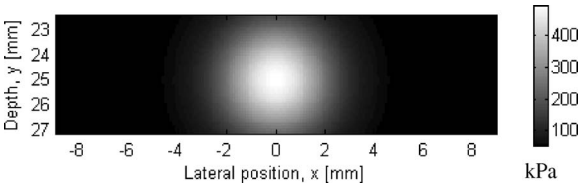

Fig. 4. Young's modulus distribution.

twice-1-D scheme. Indeed, in a twice-1-D scheme, the displacement that occurs in the direction perpendicular to the direction of estimation hinders the possibility of correctly estimating the displacement. Thus, the variation of the acoustic signature perpendicular to the estimation direction has to have a slow variation. This is the reason why two sets of images are used, as in [16], where a heterodyning demodulation scheme has been used. This demodulation method introduced in [19] a refinement of the estimation method presented by Jensen and Munk in [20]. It provides images with only lateral oscillations. This demodulation technique is based on the combination of even and odd images obtained in our work by Hilbert transform in the axial or in the lateral direction. This method is also interesting because it enables us to multiply by a factor of two the lateral oscillations frequency. Those images are used for the lateral estimation. For the images for axial estimation, a conventional beamformer is well adapted. This approach is illustrated graphically in Fig. 3.

IV. Simulation Result

A. Parameters of the Medium

The displacement vector estimation method has been applied to simulated data to show quantitatively the improvement due to the specific lateral PSF profile given in (11). The medium simulated is two-dimensional inside the image plane. The medium is considered to be 10 mm deep and located at a depth between 20 and 30 mm. The Poisson's ratio of the medium is assumed equal to 0.49 and the Young's modulus distribution is given in (19) and shown in Fig. 4.

The background value of Young's modulus is equal to 50 kPa. Located in the middle is an inclusion having a Gaussian distribution reaching a maximum of 500 kPa. This leads to the following expression of Young's modulus:

$$E = 50 + 450e^{-\pi\left(\frac{x}{4}\right)^2} e^{-\pi\left(\frac{(y-25)}{4}\right)^2}. \tag{19}$$

The maximum elasticity contrast is a factor of 10. The medium is compressed in the axial dimension. An axial displacement of 0.3 mm is applied to the edge of the phantom situated at 30-mm depth. Following convention, the point that is taken as reference (zero displacement) is located at the middle of the phantom.

The displacement map inside the phantom was calculated using FEMLAB (Ver 3.1., COMSOL AB, Stockholm,

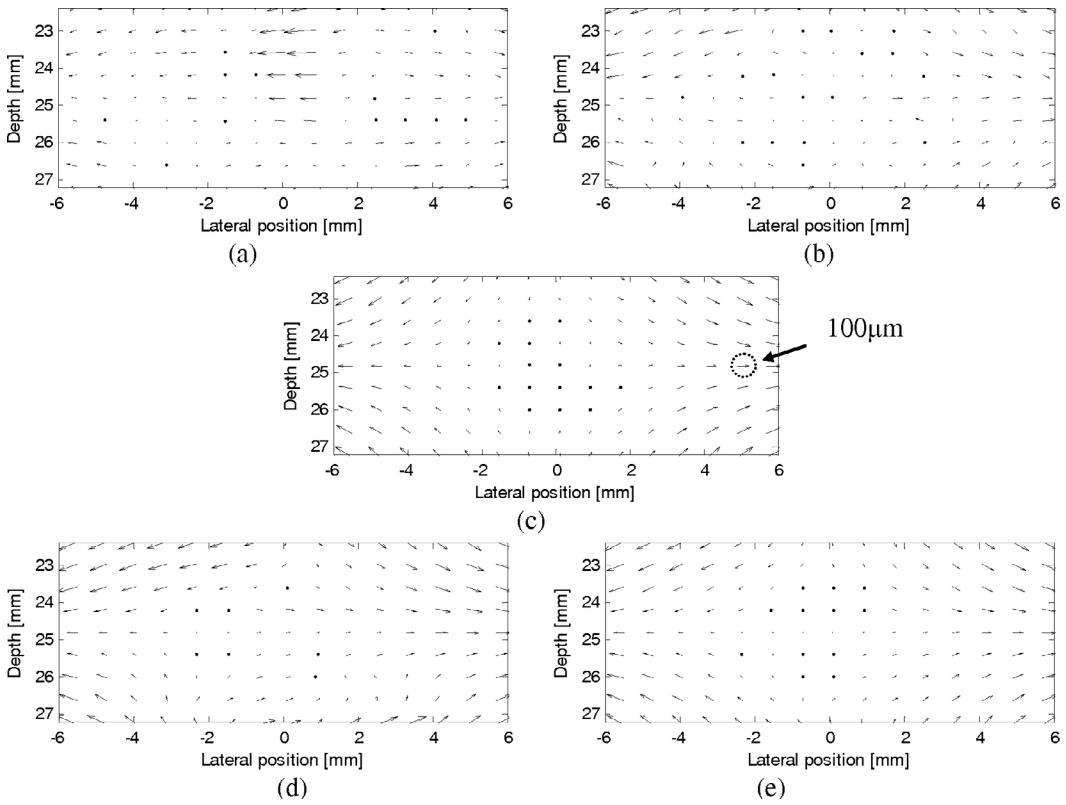

Fig. 5. (c) True displacement; (a) displacement estimated from conventional images by speckle tracking, (b) from dedicated images with speckle tracking, (d) from conventional images with the twice-1-D method, and (e) from dedicated images with twice-1-D method. The arrows scale is indicated for the circled arrow which is 100 μm.

Sweden). The reference and strain ultrasound images were calculated using (1), the convolution between the distribution of scatterers and the analytical expression of the PSF. For the conventional images, the expression of the PSF is

$$h(x,y) = e^{-\pi\left(\frac{x}{\sigma_x}\right)^2} e^{-\pi\left(\frac{y}{\sigma_y}\right)^2} \cos\left(2\pi\frac{y}{\lambda_y}\right), \tag{20}$$

with $\lambda_y = 0.2$ mm, $\sigma_y = 0.8$ mm, and $\sigma_x = 1.4$ mm. For the images with lateral oscillations, the PSF is

$$h(x,y) = e^{-\pi\left(\frac{x}{\sigma_x}\right)^2} e^{-\pi\left(\frac{y}{\sigma_y}\right)^2} \cos\left(2\pi\frac{x}{\lambda_x}\right)\cos\left(2\pi\frac{y}{\lambda_y}\right), \tag{21}$$

with $\lambda_y = 0.2$ mm, $\sigma_y = 0.8$ mm, $\lambda_x = 2.6$ mm, and $\sigma_x = 2.8$ mm. The density of scatterers was 34.5 scatterers/mm^2, which corresponds to 1.38 scatterers/λ_y^2. The displacement vector estimation method of Fig. 3 was used to estimate the axial and lateral displacement maps.

In order to show the improvement in lateral displacement estimation due to the use of our specific images with lateral oscillations, we have also used our method with only conventional images for both directions of estimation. For both cases, the same estimation method has been used (case 1: conventional images for both directions of estimation; case 2: conventional images for axial estimation and lateral oscillating images for lateral estimation). Finally, in order to give a comparison of the result of our method compared to a well-known method, we have also tested a classical speckle tracking algorithm based on the maximization of the normalized 2-D cross-correlation function. The results are given in the following section.

B. Results

The true and estimated 2-D displacement vectors are shown in Fig. 5, while the lateral displacement maps are provided in Fig. 6. The histograms of the error for the lateral displacement are given in Fig. 7. With conventional images and speckle tracking, the standard deviation of the error distribution is 150.3 μm; with dedicated images and speckle tracking, it is 71.2 μm; with conventional images and twice-1-D method, it is 37.1 μm; and with dedicated images and twice-1-D method, it is 11.4 μm.

V. Experimental Result

A. Experimental Setup and Approach

Our laboratory is well experienced in the construction of phantoms dedicated to elastography by use of a material called polyvinyl alcohol (PVA) Cryogel [21]. The stiffness of this material can be controlled by subjecting it to different numbers of freeze/thaw cycles. For our study, a parallelepiped-shaped phantom with a hard cylindrical in-

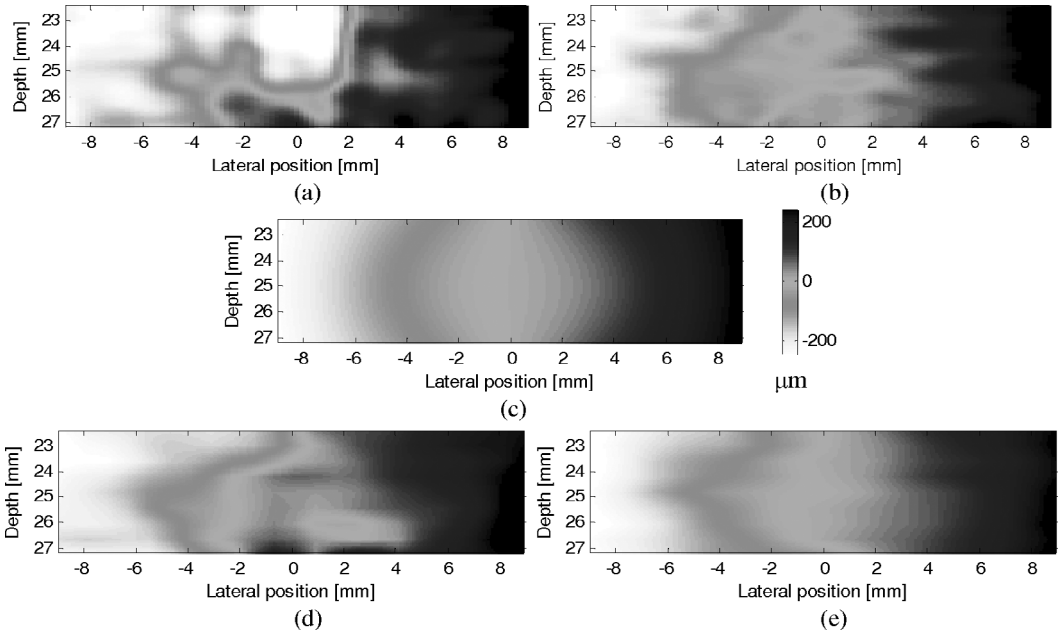

Fig. 6. (c) True lateral displacement map; (a) estimated map with conventional images by speckle tracking, (b) with dedicated images and speckle tracking, (d) with conventional images and twice-1-D method, and (e) with dedicated images and twice-1-D method.

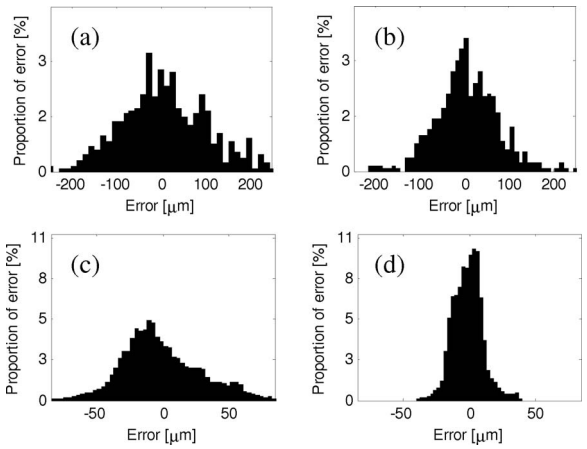

Fig. 7. Histograms of the error between true and estimated lateral displacement (a) estimated with conventional images and speckle tracking, (b) with dedicated images and speckle tracking, (c) with conventional images and twice-1-D method, and (d) with dedicated images and twice-1-D method.

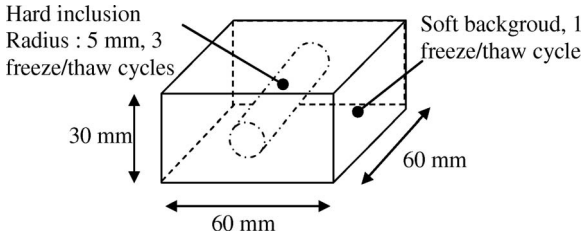

Fig. 8. Geometric configuration of the Cryogel phantom.

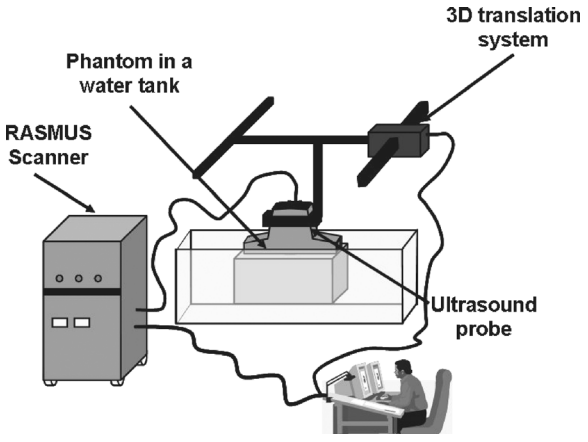

Fig. 9. Experimental setup.

clusion in its middle was constructed. The geometry and elastic properties of the phantom are given in Fig. 8.

Acquisition of the ultrasound data was made with the remote accessible multichannel ultrasound system (RASMUS) at the Center for Fast Ultrasound Imaging (CFU, Ørsted DTU, Denmark). This ultrasound scanner is dedicated to research in beamforming and synthetic aperture and is presented in detail in a recent paper by Jensen *et al.* [22]. The scanner allows nearly complete digital control of the emission as well as storage of all raw data from all transducer elements for subsequent (off-line) beamforming.

The experimental setup is shown in Fig. 9. It consists of the RASMUS scanner and a 3-D translation system, both fully operated from the user PC via MATLAB (The MathWorks, Inc., Natick, MA). The phantom and the tip of the transducer are immersed in a water tank. The user can apply any kind of displacement to the probe by means of the 3-D translation system. Two experiments were carried out.

First, the possibility of estimating a pure lateral displacement was tested. The aim was to evaluate the lateral

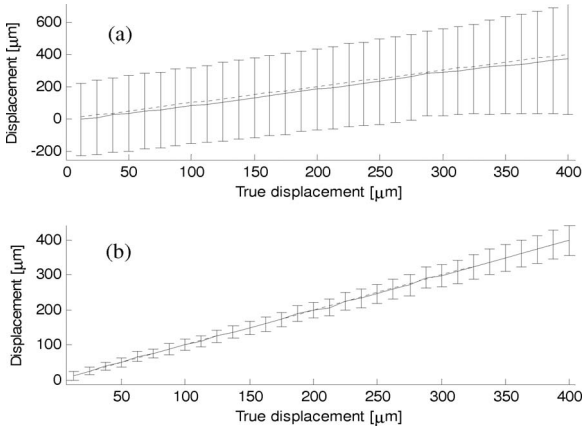

Fig. 10. Displacement estimated in the case of a pure lateral translation with (a) conventional and (b) dedicated images.

displacement estimation without having axial displacement that could decrease the quality of the estimation. Here, the ultrasound probe was translated in a direction parallel to the surface of the phantom. No compression was applied. The phantom was standing still on the bottom of the water tank.

In the second experiment, the phantom was compressed with the probe to have axial and lateral displacement. No compression plate was used. The phantom was unfixed on the lateral boundaries. Those acquisitions were used to test the whole displacement vector estimation method.

For those experiments, the raw data received from each element were acquired and the sketch of Fig. 3 was used. A plane wave was produced in emit; conventional beamforming in receive was used for producing the conventional images, and specific beamforming in receive for the dedicated images with lateral oscillations.

In order to have an idea of the displacement map that should be obtained, a finite element simulation was done with the geometry of Fig. 8. The result of this simulation should be interpreted with caution because the exact Young's modulus of the medium (phantom and inclusion) as well as the Poisson's ratio are not known exactly. However, this simulation gives a good idea of the progress reached thanks to our method.

B. Experiment One: Lateral Displacement Only

The first step was the acquisition of a reference image. Then the probe was translated laterally in steps of 25 μm. The estimation of the lateral displacement was then carried out between each of those subsequent images and the reference image. Both the reference image and the subsequent images were divided into lateral 1-D windows of length 6 mm, with a 90% overlapping between the windows, and the estimation was done for all windows. The result reported in Fig. 10 shows the mean estimate and standard deviation between each pair of images. This was carried out for conventional (a) and dedicated (b) images. The standard deviation is always 7 times smaller with dedicated images than with conventional images. For a displacement to be estimated at 50 μm, 200 μm and 350 μm, the standard deviations are 230 μm, 252 μm, and 298 μm, respectively, for conventional images, and 12 μm, 23 μm, and 37 μm, respectively, for the dedicated images. The ratio between the standard deviation and the displacement to be estimated gets smaller for large displacements, which indicates a smaller relative error for large displacements.

C. Experiment Two: Axial and Lateral Displacement

One image was acquired before compression and one after applying an axial displacement of 150 μm. Before applying this small displacement, a pre-compression of 10% of the height of the phantom was applied to ensure a good contact between the probe and the phantom.

The displacement vectors estimated for conventional and for dedicated images are represented in Fig. 11. In this section, the axial and lateral displacement maps are estimated the same way as for the simulated images, using the block diagram given in Fig. 3. The lateral displacement maps are also presented in Fig. 12.

VI. Discussion

A Newton method has been used for estimating the zero crossing of the phase of the complex correlation between 1-D windows extracted from the lateral direction of the RF ultrasound images. The use of this particular estimator has led us to design a receive beamformer resulting in dedicated images with lateral oscillations. To obtain an estimate of the displacement vector, the same estimation is used for each direction in a twice-1-D scheme. Two sets of images are used, one for each direction of estimation.

The improvement of the precision due to the use of dedicated images for lateral displacement estimation is well illustrated in simulation. First, the arrow representation of Fig. 5 gives a qualitative impression of this improvement. When conventional images are used, the estimation vectors appear different from those of the true displacement arrows, whereas with dedicated images, the errors can hardly be seen. This can also be seen in Fig. 6 where only the lateral component of the displacement is represented. Here the map estimated from dedicated images is more regular and closer to the true one. This shows that with dedicated images having lateral oscillations, there are fewer errors than with conventional images, even if some errors can still be found with the dedicated images. This can also be seen in Fig. 7 which shows the histograms of the lateral displacement error. With conventional images, the standard deviation of the error distribution is 37.1 μm and for lateral oscillations it is 11.4 μm. This represents an improvement of more than a factor of 3.

We have also tested a conventional speckle tracking algorithm with both kinds of images, the conventional ones and the ones with lateral oscillations. This method does not give as good results as the method based on the phase zero crossing, as can be seen in Figs. 5 and 6, where dif-

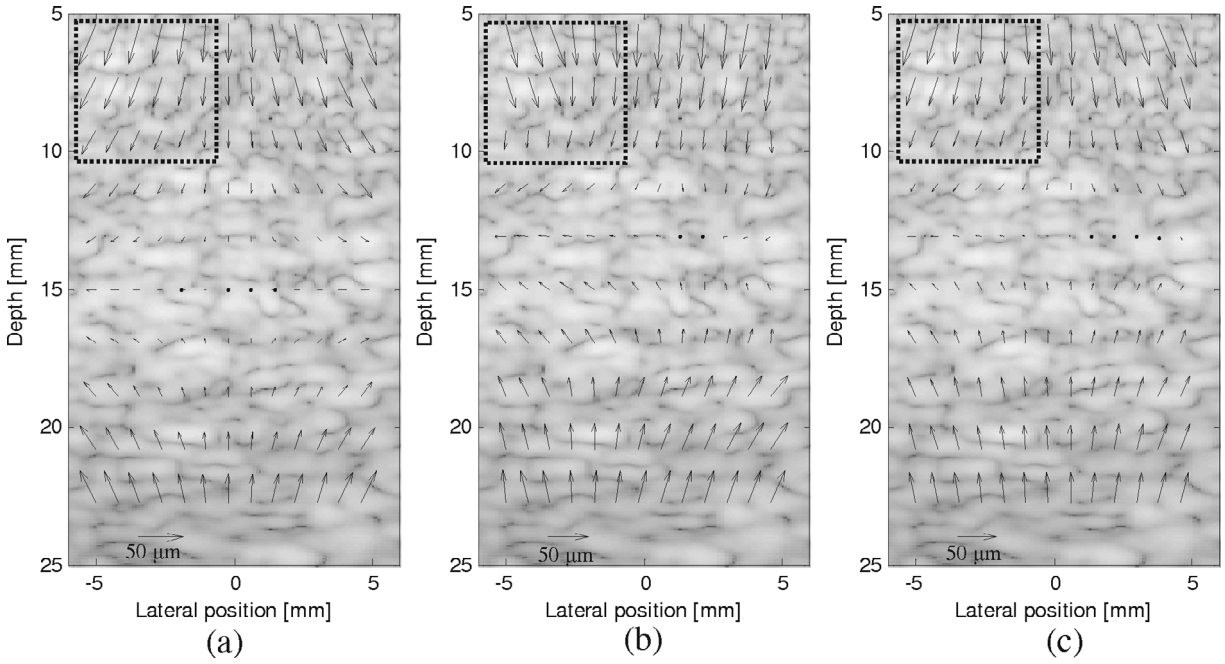

Fig. 11. Displacement vector superimposed on the associated B-mode image of the phantom, (a) from finite element simulation, and estimated (b) with conventional and (c) with dedicated images. Dotted regions highlight differences. The displacement arrows scale is given by the axial and lateral arrows of 50 μm in the left bottom corner of (a), (b), and (c).

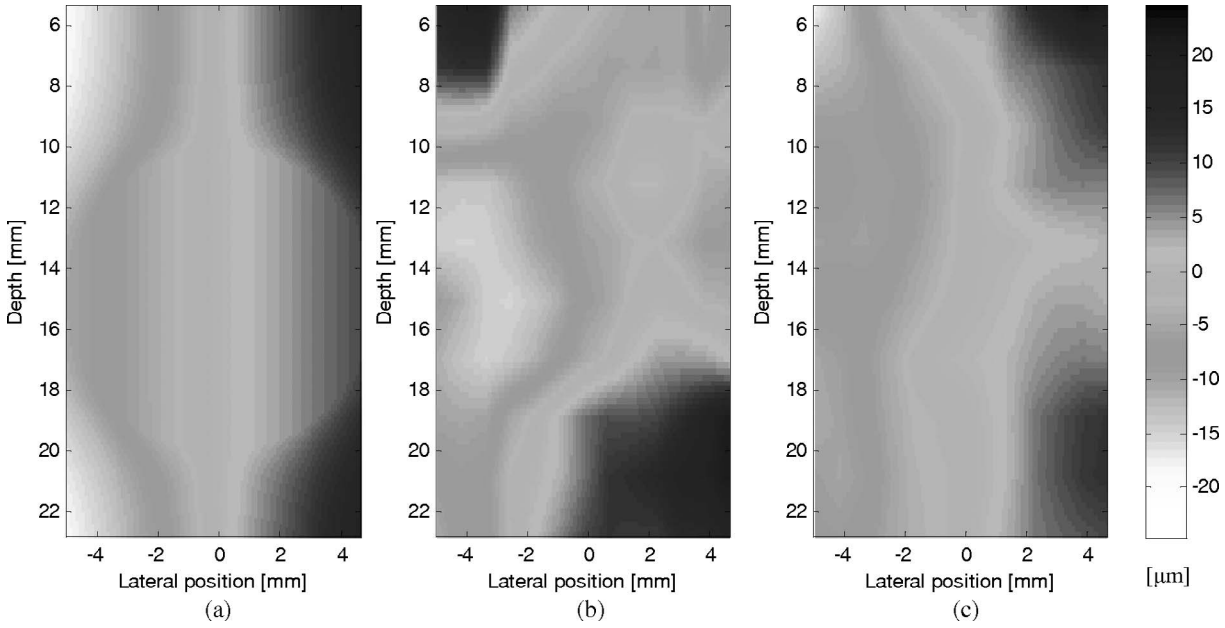

Fig. 12. (a) Lateral displacement map obtained by finite element simulation, and estimated (b) with conventional and (c) with dedicated images obtained with experimental data.

ferences appear more clearly for the speckle tracking technique than for our technique. An interesting result concerns the fact that lateral oscillations also improve the lateral estimation result in the case of speckle tracking. This is probably due to the fact that higher frequencies are present in the lateral direction of the images, leading naturally to an easier bloc matching. The histograms of Fig. 7 show that, for lateral oscillations, our method based on the phase leads to a standard deviation of the error which is around 7 times smaller than with speckle tracking.

The experimental feasibility of the method has been investigated in two steps. First, the lateral displacement is estimated when only a lateral translation is present between the acquisitions. Again, a comparison between the estimation obtained with conventional images and the one obtained with dedicated images is given in Fig. 10. The improvement due to the lateral oscillations leads to a smaller

error between the estimate and the true value. The estimated curve fits better than the true one. Moreover, the standard deviation is always 7 times smaller with dedicated images than with conventional images.

The method was finally tested with a real phantom built with PVA Cryogel. The medium contains a hard inclusion in its middle. The lateral displacement map obtained with conventional images and the one obtained with dedicated images are given in Figs. 11 and 12. A finite element simulation was done in order to reproduce the experimental conditions. As the exact elastic properties of the Cryogel phantom are not known, the true displacement map is not known. However, it gives a good idea of the coherence of the results. Particularly, some ill-estimated points are present in the result obtained with conventional images, inside the dotted regions. Specifically, if the compression is applied in the middle of the phantom, the lateral displacement should be in the direction of the edges, and not toward the middle of the phantom, which is the case here in Fig. 11(b). This leads us to the conclusion that there is a real improvement due to the use of dedicated images which give a smoother displacement map.

It is important to keep in mind that there is a limit to how much the beamforming parameters can be optimized. This limit is fixed by the size of the ultrasound probe. The two key parameters of the PSF are the lateral oscillations wavelength, which is related to the complex correlation phase slope and the estimation's precision, and the width of its Gaussian envelopes, which is related to the spatial resolution of the images. The optimal values according to our probe are deduced from Fig. 2. This figure shows that the results could be increased even more, if smaller parameters could be used.

The estimation could probably be as good for both directions of space if the same oscillations frequency could be reached in the lateral and in the axial direction. First, it is important to notice that this can be reached only after heterodyning demodulation, which decreases by a factor of two the lateral wavelength. The problem is that with the beamforming method chosen, it is possible to change only the receive beamforming. With the same element's size, this would lead to a probe of 600 elements. An improvement can probably be reached by using a synthetic aperture and changing the emit PSF profile.

VII. Conclusions

In this paper we have presented the design of a PSF dedicated to lateral displacement estimation for ultrasound tissue elasticity imaging.

As the estimation method chosen uses the phase of the complex correlation between signals from the lateral direction of the ultrasound RF images, the phase of this complex correlation function is forced to be linear. The consequences for the shape of the lateral signals and for the PSF have been derived analytically. The lateral profile of the PSF shows oscillations as in the axial direction of a conventional PSF.

A comparison with conventional PSF has been evaluated quantitatively in simulations and experimentally. Thanks to the dedicated PSF, an increase in the accuracy of the estimation has been highlighted with an important diminution of the standard deviation of the error (between a factor of 3 and a factor of 7, depending on the situation).

The precision of the method can probably still be increased. However, it would necessitate a larger ultrasound probe or another beamforming approach, e.g., a synthetic aperture.

Acknowledgments

The authors thank the reviewers for their thoughtful comments.

References

[1] Y. Yamakoshi, J. Sato, and T. Sato, "Ultrasonic imaging of internal vibration of soft tissue under forced vibration," *IEEE Trans. Ultrason., Ferroelect., Freq. Contr.*, vol. 37, pp. 45–53, 1990.

[2] V. Dutt, R. R. Kinnick, and J. F. Greenleaf, "Acoustic shear wave displacement measurement using ultrasound," in *Proc. IEEE Ultrason. Symp.*, vol. 2, 1996, pp. 1185–1188.

[3] S. Catheline, J.-L. Thomas, F. Wu, and M. A. Fink, "Diffraction field of a low frequency vibrator in soft tissues using transient elastography," *IEEE Trans. Ultrason., Ferroelect., Freq. Contr.*, vol. 46, pp. 1013–1019, 1999.

[4] S. Catheline, F. Wu, and M. Fink, "A solution to diffraction biases in sonoelasticity: The acoustic impulse technique," *J. Acoust. Soc. Amer.*, vol. 105, pp. 2941–2950, 1999.

[5] J. Ophir, I. Césepedes, H. Ponnekanti, Y. Yazdi, and X. Li, "Elastography: A quantitative method for imaging the elasticity of biological tissues," *Ultrason. Imag.*, vol. 13, pp. 111–134, 1991.

[6] T. A. Krouskop, T. M. Wheeler, F. Kallel, B. S. Garra, and T. Hall, "Elastic moduli of breast and prostate tissues under compression," *Ultrason. Imag.*, vol. 20, pp. 260–274, 1998.

[7] A. Lyshchik, T. Higashi, R. Asato, S. Tanaka, J. Ito, M. Hiraoka, A. B. Brill, T. Saga, and D. K. Togashi, "Elastic moduli of thyroid tissues under compression," *Ultrason. Imag.*, vol. 27, pp. 101–111, 2005.

[8] P. E. Barbone and J. C. Bamber, "Quantitative elasticity imaging: What can and cannot be inferred from strain images," *Phys. Med. Biol.*, vol. 47, pp. 2147–2164, 2002.

[9] E. Konofagou and J. Ophir, "A new elastographic method for estimation and imaging of lateral displacements, lateral strains, corrected axial strains and Poisson's ratios in tissues," *Ultrasound Med. Biol.*, vol. 24, pp. 1183–1199, 1998.

[10] N. Nitta and T. Shina, "A method of tissue estimation based on three-dimensional displacement vector," *Jpn. J. Appl. Phys.*, vol. 39, pp. 3225–3229, 2000.

[11] M. Tanter, J. Bercoff, L. Sandrin, and M. Fink, "Ultrafast compound imaging for 2-D motion vector estimation: Application to transient elastography," *IEEE Trans. Ultrason., Ferroelect., Freq. Contr.*, vol. 49, pp. 1363–1374, 2002.

[12] A. Pesavento, C. Perrey, M. Krueger, and H. Ermert, "A time-efficient and accurate strain estimation concept for ultrasonic elastography using iterative phase zero estimation," *IEEE Trans. Ultrason., Ferroelect., Freq. Contr.*, vol. 46, pp. 1057–1067, 1999.

[13] X. Chen, M. J. Zohdy, S. Y. Emelianov, and M. O'Donnell, "Lateral speckle tracking using synthetic lateral phase," *IEEE Trans. Ultrason., Ferroelect., Freq. Contr.*, vol. 51, pp. 540–550, 2004.

[14] J. C. Bamber and R. J. Dickinson, "Ultrasonic B-scanning: A computer simulation," *Phys. Med. Biol.*, vol. 25, pp. 463–479, 1980.

[15] R. F. Wagner, S. W. Smith, J. M. Sandrik, and H. Lopez, "Statistics of speckle in ultrasound B-scans," *IEEE Trans. Sonics Ultrason.*, vol. 30, pp. 156–163, 1983.
[16] H. Liebgott, J. Fromageau, J. Wilhjelm, D. Vray, and P. Delachartre, "Beamforming scheme for 2D displacement estimation in ultrasound imaging," *EURASIP J. Appl. Signal Process.*, vol. 2005, pp. 1212–1220, 2005.
[17] J. A. Jensen and P. Munk, "A new method for estimation of velocity vectors," *IEEE Trans. Ultrason., Ferroelect., Freq. Contr.*, vol. 45, pp. 837–851, 1998.
[18] M. Anderson, "Multi-dimensional velocity estimation with ultrasound using spatial quadrature," *IEEE Trans. Ultrason., Ferroelect., Freq. Contr.*, vol. 45, pp. 852–861, 1998.
[19] M. E. Anderson, "A heterodyning demodulation technique for spatial quadrature," in *Proc. IEEE Ultrason. Symp.*, vol. 2, 2000, pp. 1487–1490.
[20] J. A. Jensen and P. Munk, "Improved estimation and focusing scheme for vector velocity estimation," in *Proc. IEEE Ultrason. Symp.*, vol. 2, 1999, pp. 1465–1470.
[21] J. Fromageau, E. Brusseau, D. Vray, G. Gimenez, and P. Delachartre, "Characterization of PVA cryogel for intravascular ultrasound elasticity imaging," *IEEE Trans. Ultrason., Ferroelect., Freq. Contr.*, vol. 50, pp. 1318–1324, 2003.
[22] J. A. Jensen, O. Holm, L. J. Jensen, H. Bendsen, S. Nikolov, B. G. Tomov, P. Munk, M. Hansen, K. Salomonsen, J. Hansen, K. Gormsen, H. M. Pedersen, and K. L. Gammelmark, "Ultrasound research scanner for real-time synthetic aperture data acquisition," *IEEE Trans. Ultrason., Ferroelect., Freq. Contr.*, vol. 52, pp. 881–891, 2005.

Jørgen Arendt Jensen (M'93–SM'02) earned his M.S. degree in electrical engineering in 1985 and the Ph.D. degree in 1989, both from the Technical University of Denmark. He received the Dr.Techn. degree from the university in 1996. He has published more than 140 journal and conference papers on signal processing and medical ultrasound and the book, *Estimation of Blood Velocities Using Ultrasound*, Cambridge University Press, in 1996. He is also developer of the Field II simulation program. He has been a visiting scientist at Duke University, Stanford University, and the University of Illinois at Urbana-Champaign. He is currently full professor of Biomedical Signal Processing at the Technical University of Denmark at Ørsted•DTU and head of Center for Fast Ultrasound Imaging. He is also adjunct full professor at the Faculty of Health Sciences at the University of Copenhagen. He has given courses on blood velocity estimation at both Duke University and the University of Illinois and teaches biomedical signal processing and medical imaging at the Technical University of Denmark. He has given several short courses on simulation, synthetic aperture imaging, and flow estimation at international scientific conferences. He has received several awards for his research. He is also the co-organizer of a new biomedical engineering education program offered by the Technical University of Denmark and the University of Copenhagen. His research is centered around simulation of ultrasound imaging, synthetic aperture imaging and blood flow estimation, and constructing systems for such imaging.

Hervé Liebgott earned the M.Sc. degree in electrical engineering and in acoustics from the INSA de Lyon in 2002 and the Ph.D. degree in acoustics from the INSA de Lyon in 2005. He is currently associate professor at Université Claude Bernard Lyon 1 where he teaches in the department GEII from the IUT B. His research deals with signal processing applied to ultrasound imaging.

Didier Vray (M'92) was born in Saint-Etienne, France, in 1959. He received his B.S.E. degree in electrical engineering from Saint-Etienne University in 1981 and his M.S. degree in applied computer sciences from the Institut National des Sciences Appliquées (INSA), Lyon, France, in 1984. He received the Ph.D. degree from INSA-Lyon in 1989 for a work in acoustics and signal processing. He is currently a professor of Signal Processing and Computer Sciences at INSA-Lyon. Since he joined the research laboratory CREATIS, his main research interests have included ultrasound medical imaging, elastography, and high frequency imaging.

Jens E. Wilhjelm (S'86–M'86–S'88–M'91) earned the M.Sc. degree in electrical engineering from the Technical University of Denmark in 1986 and the Ph.D. degree in biomedical engineering in 1991 from Worcester Polytechnic Institute, Worcester, MA. From 1986 to 1988, he worked with blood flow measurements in the ultrasonic laboratory at Brüel & Kjær A/S, Nærum, Denmark. In 1991, he came to the Electronics Institute, Technical University of Denmark where he held various fellowship positions until he became an associate professor in 1997 at the Department of Information Technology (now Ørsted DTU). His current research interests in medical diagnostic ultrasound include technical and medical aspects within classification of atherosclerotic plaque, signal processing, and Doppler based blood flow measurements.

Philippe Delachartre received his M.S. degree in 1990 and a Ph.D. degree in 1994, both in signal and image processing in acoustics from the National Institute for Applied Sciences of Lyon (INSA-Lyon, France). Since 1995, he has worked as an associate professor at the Electrical Engineering Department of the INSA-Lyon and researcher at the Center for Research and Applications in Image and Signal Processing (CREATIS). His research interests include the image formation modeling and the parametric imaging applied to the field of medical ultrasound imaging.